


**LETTER**

# Electrical impedance tomography image reconstruction for lung monitoring based on ensemble learning algorithms<sup>1</sup>

Areen K. Al-Bashir<sup>1</sup>  | Duha H. Al-Bataiha<sup>1</sup> | Mariem Hafsa<sup>2</sup> |  
Mohammad A. Al-Abed<sup>2</sup> | Olfa Kanoun<sup>3</sup>

<sup>1</sup>Biomedical Engineering Department, Jordan University of Science and Technology, Irbid, Jordan

<sup>2</sup>Biomedical Engineering Department, Hashemite University, Zarqa, Jordan

<sup>3</sup>Measurement and Sensor Technology, Chemnitz University of Technology, Chemnitz, Germany

**Correspondence**

Areen K. Al-Bashir, Biomedical Engineering Department, Jordan University of Science and Technology, P. O. Box 3030, Irbid 22110, Jordan.  
Email: akbashir@just.edu.jo

**Funding information**

Saxon Development Bank "SAB", Grant/Award Number: 2420156; German Academic Exchange Service (DAAD); Federal Ministry for Economic Cooperation and Development (BMZ) Germany; "Promotion of Higher Education in Biomedical Engineering (PROFILE)", Grant/Award Number: 57612192; Deutscher Akademischer Austausch Dienst Kairo

**Abstract**

Electrical impedance tomography (EIT) is a promising non-invasive imaging technique that visualizes the electrical conductivity of an anatomic structure to form based on measured boundary voltages. However, the EIT inverse problem for the image reconstruction is nonlinear and highly ill-posed. Therefore, in this work, a simulated dataset that mimics the human thorax was generated with boundary voltages based on given conductivity distributions. To overcome the challenges of image reconstruction, an ensemble learning method was proposed. The ensemble method combines several convolutional neural network models, which are the simple Convolutional Neural Network (CNN) model, AlexNet, AlexNet with residual block, and the modified AlexNet model. The ensemble models' weights selection was based on average technique giving the best coefficient of determination ( $R^2$  score). The reconstruction quality is quantitatively evaluated by calculating the root mean square error (RMSE), the coefficient of determination ( $R^2$  score), and the image correlation coefficient (ICC). The proposed method's best performance is an RMSE of 0.09404, an  $R^2$  score of 0.926186, and an ICC of 0.95783 using an ensemble model. The proposed method is promising as it can construct valuable images for clinical EIT applications and measurements compared to previous studies.

## 1 | INTRODUCTION

Medical imaging technology is the process of noninvasively visualizing various tissues and organs of the human body [1, 2]. With the rapid advancement of scientific instrumentation and imaging modality, various imaging technology modalities emerged that are widely used in clinical medicine [3, 4]. Magnetic resonance imaging (MRI), ultrasound, and X-ray computed tomography (CT) are the most used imaging modalities. These modalities have matured and extensive application in the clinical setting, yet they still have some notable drawbacks. X-ray radiography and CT, for example, employ ionizing radiation, which is readily absorbed by human tissues and causes harm for prolonged exposure, especially for clinical operators [4, 5]. MRI imaging, on the other hand, takes a long time, is expensive,

and requires specialized magnetic containment [5, 6]. Moreover, ultrasound is notorious for its low-spatial resolution images and videos [6, 7]. To compensate for the downsides of conventional medical imaging technology, researchers have started to investigate other imaging techniques as alternative diagnostic tools.

Electrical impedance tomography (EIT) emerged as a promising alternative over the last couple of decades. EIT technology also has promising applications in chemical, petroleum, surface geophysical exploration, material engineering, and other fields [7, 8]. Moreover, EIT has many medical applications including brain and breast tumor imaging, lung reconstruction, and cancer detection [8, 9]. Despite having a low spatial resolution, EIT images have a high temporal resolution, making this technology essential and promising in many fields [9, 10]. In addition, electrical impedance tomography (EIT) is non-invasive, low-cost, real-time, does not use ionizing radiation, and does not require specialized housing [10, 11].

The work was conducted at Jordan University of Science and Technology and Chemnitz University of Technology.

This is an open access article under the terms of the [Creative Commons Attribution-NonCommercial-NoDerivs](https://creativecommons.org/licenses/by-nc-nd/4.0/) License, which permits use and distribution in any medium, provided the original work is properly cited, the use is non-commercial and no modifications or adaptations are made.

© 2024 The Authors. *Healthcare Technology Letters* published by John Wiley & Sons Ltd on behalf of The Institution of Engineering and Technology.

EIT systems require the integration of both hardware and software [11, 12]. The hardware includes the data acquisition system, frequency generator, current generator, and signal conditioner [12, 13]. EIT systems use electrodes placed on the targeted object's surface. The boundary voltages that appear on the surface of the electrodes, resulting from the injected signal are used to determine the inner conductivity distribution. The software component is a hybrid of two processes: The forward problem and the inverse problem [13, 14]. The forward problem compromises the design of the geometry of the measured medium [14]. Solving the forward problem is to theoretically calculate the voltage variation after the current injection procedure [15]. The second part is the inverse problem in which a complete image is reconstructed [15]. Mathematically, the EIT inverse problem is characterized as an ill-posed and nonlinear problem [16]. This means that a small difference in measurements can significantly impact the reconstructed image, and there is no single solution (image in this case) for a given potential border distribution. Therefore, in the past few decades, the image reconstruction algorithm emerged as the most important component of EIT. The characteristic of the reconstructed image is primarily determined by the accuracy of the boundary data and proposed reconstruction algorithm [16].

Traditional algorithms for image reconstruction are classified as either non-iterative or iterative [17]. Sensitivity coefficient, back projection (BP) [18], and Tikhonov regularization methods [19] are examples of non-iterative algorithms. Conjugate gradient [20], landweber [21], Kalman filtering algorithms, and Gauss Newton [22] are examples of iterative algorithms. These traditional algorithms tend to settle for a local minimum solution [23]. As a result, artifacts are produced during the image reconstruction process [23, 24].

A more contemporary optimization technique is particle swarm optimization (PSO) [17], which produces greater convergence results when training an artificial neural network (ANN) for function approximation when compared to classical backpropagation. An algorithm for stochastically global optimization is PSO. It has been demonstrated that it can be used to train an ANN to tackle EIT problems and can do so with a restricted number of repetitions.

Also, genetic algorithms (GAs) [25] have been widely used to solve optimization searching problems. When the closed-form optimization technique is not applicable, they are helpful. GAs are global search strategies that run in parallel and mimic natural genetic operators. A GA is more likely to converge toward the global solution since it assesses numerous locations in the parameter space simultaneously. It can also repeat multiple times on each incoming datum and does not require the assumption that the search space is continuous or differentiable.

Lately, neural networks and machine learning-based methods have advanced rapidly, and their strong autonomous learning ability has drawn interest from all fields. Furthermore, they are characterized by robust nonlinear approximation capacity. Neural network algorithms prevent linearizing image reconstruction, which benefits the reconstructed image's accuracy and makes them appropriate for solving the ill-posed, non-linear EIT Inverse Problem [24, 26].

A convolutional neural network (CNN) is a popular neural network model used recently for image classification, segmentation, and reconstruction problems among the various deep learning architectures [27]. CNNs' main strength is their efficient dense network for prediction or identification [28]. Several cutting-edge deep CNN architectures have been made publicly available for researchers and data scientists to use. Recently, pre-trained models, also known as transfer learning, have been developed and demonstrated to be effective. Transfer learning is a method that starts with pre-trained models and progresses to the development of neural network models for computer vision and language processing tasks that require significant computing and time resources. Transfer learning aims to improve learning by incorporating knowledge from the source task.

Nevertheless, a single learner may exhibit unsatisfactory performance due to various challenges such as falling into local minima, limited hypothesis space, and incorrect hypothesis space selection [29]. Hence, different frameworks employing ensemble CNN models have been tried to improve the accuracy of clinical decision-support systems [30].

To enhance prediction performance and overcome the drawbacks of having only one or two weak learners (base models), the ensemble learning approach was introduced. It is interesting as it combines multiple machine learning models [31]. The ensemble's basic form is an average ensemble that computes its output using the mean of base model outputs. Each base model in the average ensemble is given the same weight and strength in the computation. Because the average ensemble treats all base models equally, this could lead to an undesirable performance. On the other hand, the weighted average ensemble is a clever variation of the average ensemble that assigns weight to each model. High-accuracy base models are allocated weights higher than others, which are assigned lower weights. Many expressions, such as combined, hybrid, integrated, and aggregated have been used in the literature to describe ensemble learning [32]. Several studies have shown empirical evidence that ensemble learning performs better than individual learners in terms of prediction accuracy [33–35]. Ensemble methods are broadly categorized into two types of base learner forms: (1) homogeneous ensemble methods and (2) heterogeneous ensemble methods [32]. In homogenous ensemble methods, identical base learners are applied to a different set of instances in a dataset. Conversely, various machine-learning techniques in the heterogeneous ensemble method generate an assortment of base learners. In both cases, these base learners are combined, and the results are predicted by statistically or democratically integrating the base learners' outcomes [36]. Because of the different natures of base learners, heterogeneous methods are more diverse than homogeneous methods. Moreover, Ensemble methods are also classified as linear or nonlinear. The result of base learner models is aggregated using a linear function, such as a simple average or weighted average, in linear ensemble systems. In contrast, in non-linear ensemble methods, a non-linear approach, such as a support vector machine (SVM) or decision tree, is used to integrate base learner decisions [37].

The scientific and medical fields have paid close attention to the growth of ensemble learning techniques and methodologies over the last few decades [38]. Along these lines, several ensemble learning techniques have been proposed and used in the regression and classification of real-world problems [39]. Previous studies have used ensemble approaches with remarkable results for improving medical diagnosis and decision-making [40]. The authors of [41] investigated disease prediction using a multi-layer classifier. The model produced significant results on publicly available disease datasets and was used to aid in medical decision-making. Moreover, a well-performing homogeneous ensemble learning model based on weighted averaging for the prediction of heart disease risk was discussed in [42]. The proposed approach demonstrated improved performance in effectively predicting heart disease. In addition, the work in [43] described a novel carcinoma detection methodology based on a linear and heterogeneous ensemble learning that aids in the prediction of carcinoma from CT scanned images. The proposed methodology gives an in-depth knowledge of lung cancer prediction. The authors of [44] suggested a non-linear and homogenous ensemble learning model integrated with an effective optimizer to achieve better electrical capacitance tomography (ECT) reconstructions than the advanced imaging methods. The developed algorithm reduces reconstruction error while significantly improving imaging quality and robustness. A non-linear and heterogeneous cascade ensemble that combines multiple models to improve CT image reconstruction was explained in [45]. The proposed method demonstrated improved performance for image quality metrics CT reconstruction task. Ensemble learning is primarily implemented as two sub-procedures: training weak component learners and selectively combining the member learners into stronger learners. This presents researchers with two difficult tasks: how to select learning algorithms and training data sets, and how to parameterize the selected algorithms to make the weak learners as diverse as possible; and how to conclude the learning result with varied outputs from the member learners.

In this proposed algorithm, a linearly aggregated heterogeneous method is proposed to reconstruct the EIT using a simulated dataset. The objective is to achieve robust shape reconstructions and high resolution. The ensemble method combines several CNN models: the simple CNN, AlexNet, AlexNet with residual block, and the modified AlexNet model. The work is presented as follows: Section 2 describes the network structures of the proposed ensemble method and the reconstruction process of the EIT simulation data. Then, the results and discussion are explained in Section 3. Finally, conclusions and future works are drawn in Section 4.

## 2 | METHOD

This section includes a description of the dataset, different CNN models implemented to solve the EIT problem, and the ensemble learning approach used to enhance the overall accuracy of the results.

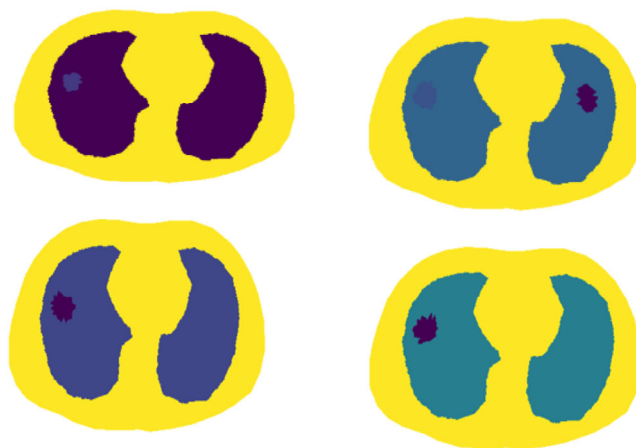


FIGURE 1 Actual distribution for different samples.

### 2.1 | EIT simulation dataset

EIT simulation models are used because actual conductivity distributions are difficult to achieve in EIT practical applications. The deformation of the chest domain and target lungs with complex conductivity distribution caused by lung diseases may be time-varying due to the respiratory operation in EIT lung reconstructions, making the EIT lung problem more difficult. Therefore, in this work, the dataset is numerically simulated as shown in Figure 1 in the professorship measurement and sensor technology (MST) at the Chemnitz University of Technology in Germany, based on a previously developed realistic thorax and lung mesh [46]. The conductivity is simulated, and the forward problem is solved to determine the boundary voltages depending on the results. The simulated dataset and the sixteen-electrode EIT model were received using the PyEIT (a Python-based package) a library for EIT processing.

The dataset includes 10,000 cases. Each case has 208 boundary voltage values including a corresponding conductivity distribution vector with 2707 elements. Each value in the truth data represents the conductivity value of one triangle in the mesh. That is where the color comes from when visualizing the image. For each image, the color bar represents the range of the conductivity change, and the numbers represent the maximum range of change.

### 2.2 | The network structure for EIT image reconstruction

As a feed-forward neural network with self-learning and high robustness ability, CNN requires fewer network parameters than other neural network models [47]. According to that, four CNN models have been implemented.

- 1) Simple CNN [48]: It has three conv1D and all of them have an Elu activation function. While a batch normalization layer follows the first two layers. The last one is followed by a max pooling layer with a kernel size of 4. The three conv1D ker-

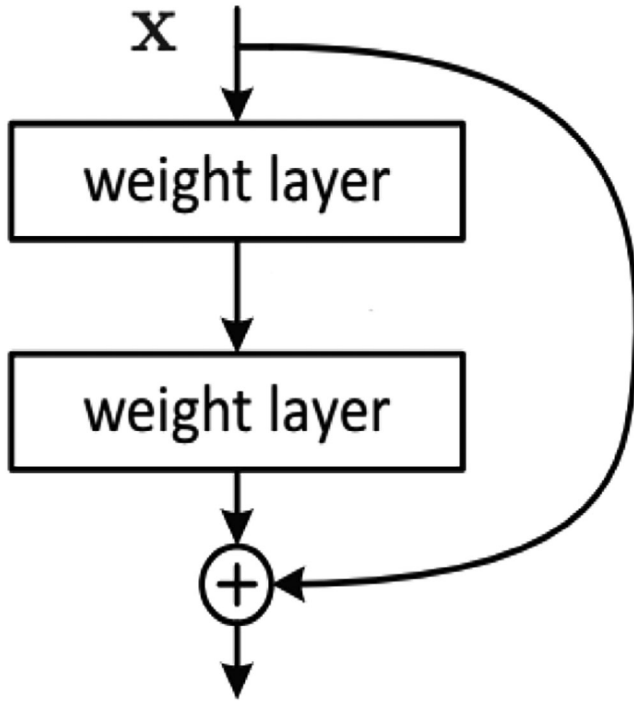


FIGURE 2 Residual block.

nel sizes are all 9 while the number of filters for each layer is 64, 128, and 56, respectively, then we added two fully connected layers. The first one has an Elu activation function. These fully connected layers have 2500, and 2707 neurons, respectively.

- 2) AlexNet [49]: the model is inspired by AlexNet architecture with some modifications to fit the needs of the used data.

An Elu activation function and a MaxPool1D function with a kernel size of two follow the first two conv1D, then we followed with two conv1D; each one has an Elu activation function, but the MaxPool1D function with a kernel size of two follows only the last one. The four conv1D have a kernel size of 11,5,3, and 3, respectively. The filter (number of channels) size of 96, 256, 384, and 256, respectively. Three fully connected layers then follow these combinations of conv1D layers; the first two have a dropout layer between them, and each one of them is followed by an Elu activation function, then we added one last fully connected layer to deliver our output from the model. The three fully connected layers have 4096, 4096, and 2707 neurons, respectively.

- 3) AlexNet with a residual block: this model is like the second model except for adding a residual block after the first conv1D layer. The residual block [50] is any number of consecutive weighted layers (mostly convolution layers) with a skip connection which adds the input to this layer to the output of the last layer as appears in Figure 2. The residual blocks allow memory (or information to flow from the initial to the last layers). In this model, the weighted layers are two layers of conv1D with a kernel size of 11 and the number of filters is 96.

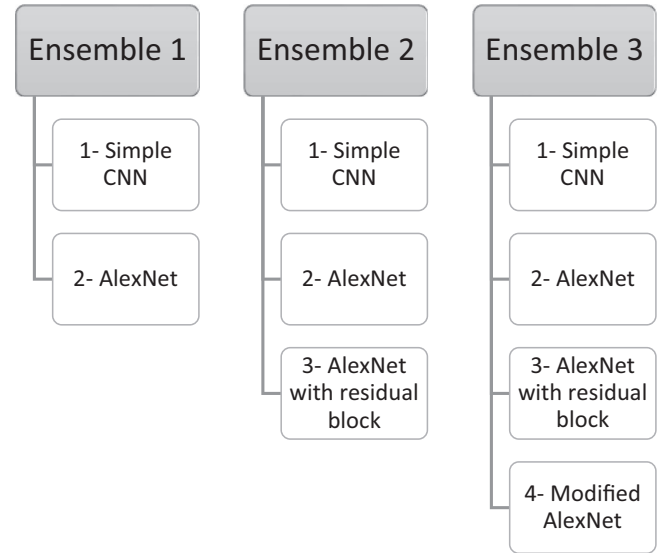


FIGURE 3 The proposed ensemble models. The technique used for all ensemble models was weighted average.

- 4) Modified AlexNet model: the last model is nearly the same as the first AlexNet model with one modification: adding a conv1D layer before the last two layers. The kernel size of this layer is 3, and the number of filters is 384.

### 2.3 | Ensemble learning method

Because of their ability to detect nonlinear correlations, machine learning algorithms are increasingly being used in a variety of medical applications [51]. Medical imaging applications use ensemble algorithms to improve prediction accuracy [52]. As previously stated, the ensemble learning method combines the decisions of different learning models to solve a problem more efficiently than using a single learning model. Based on that, a different linearly aggregated heterogeneous method using the weighted average approach for EIT image reconstruction for lung monitoring was proposed and tested. The resultant features will be fused with different voting mechanisms to obtain better results than any constituent algorithm alone. Accordingly, all the features used in the ensemble methods will be unique compared to other models.

After the completion of the implementation and training of the four CNN models, the ensemble learning method was implemented. The ensemble model takes the output of each of the four models using the following weighted average equation:

$$dotsns. = \frac{p_1 \cdot w_1 + p_2 \cdot w_2 \dots \dots p_n \cdot w_n}{w_1 + w_2 + \dots w_n}, \quad (1)$$

where  $p$  refers to the predicted value of each mode,  $w$  is a constant weight that ranges from zero to one, and  $n$  refers to the number of models.

As presented in Figure 3, several combinations were proposed in this work.



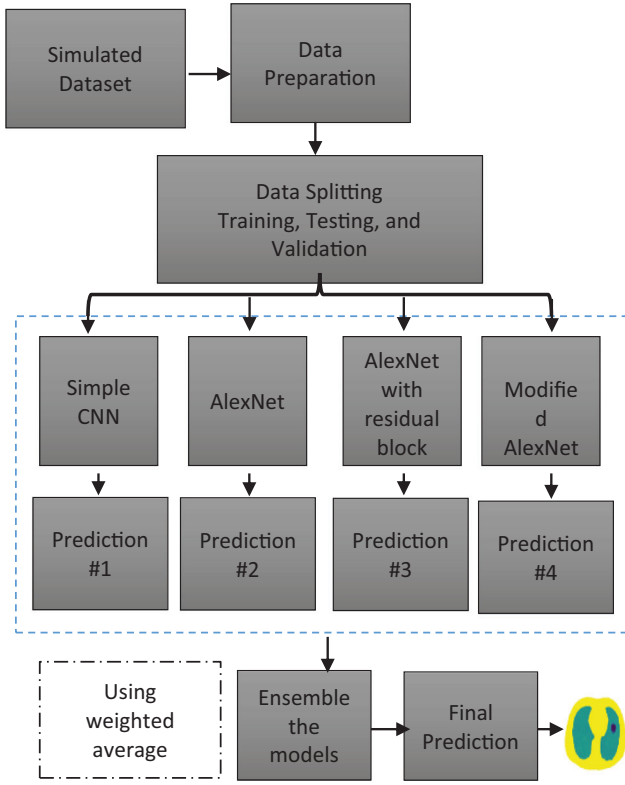


FIGURE 4 Summary of the proposed workflow.

All combinations of weights with a step of 0.1 for each weight are tried. The best combinations of weights that achieved the highest  $R^2$  score were chosen.

A summary of the proposed workflow is shown in Figure 4. This approach explains image reconstruction for EIT for lung monitoring. The proposed work, as explained in the flowchart, consisted essentially of two parts: dataset preparation and model training and testing. Firstly, a simulated dataset of EIT boundary voltages was generated and then used as an input for the work. Secondly, the data was split into 75% training and 25% validation and testing. The training set with the corresponding conductivity distribution was then entered into the model, which was then trained using a particular loss function.

After training, the trained model and weights were used to evaluate and test unseen slices; accordingly, the predicted outputs were generated and compared to the provided ground truth. If the reconstructed results were unconfirmed, the model design and/or training parameters were fine-tuned, and training was repeated until the predicted outputs were acceptable. At that point, the final model and weights were saved.

## 2.4 | Network training

The study's models were all created using the Python programming language, because it is open source and maintained by Google, it is constantly developed. Along with additional libraries, Tensorflow 2.4.1 and Keras 2.2.4 were used to train the machine learning and CNN models presented in this study.

TABLE 1 Summary of the parameters used to develop the proposed models.

Name	Value
Input neurons	208
Output neurons	2707
Batch size	75
Dataset	10,000 cases
Training set	75%
Validation set	20%
Test set	5%
Optimizer	Adam
Activation function	Elu
Cost function	MSE
Output activation function	Linear
Learning rate	0.001

Computer resource limitations have been a significant barrier throughout the research because of the quantity of the dataset and the complexity of the machine learning models. Thus, Google Colab GPU Libraries were used for all studies. All the proposed models are trained using mean square error as a loss function and Adam optimizer. The hyperparameters for the models are the same as the batch size is 75 and 25 for training and validation sets, respectively. Also, the learning rate is 0.001. Lastly, the number of epochs for each model is not a fixed number as we used the early stop function to determine when the model should stop training, as the model will stop training only if the validation loss did not decrease for 20 consecutive epochs. The model weights will only be saved when the validation loss decreases throughout the training. Validation loss is measured after each epoch to ensure that avoids overfitting on each proposed model. An overview of the used ANN parameters is shown in Table 1.

## 2.5 | Evaluation methods

A model's performance is assessed by evaluation metrics. The discrepancy between the actual values and the predicted values for the chosen model must be minimal and unbiased for the training, validation, and test datasets to ensure a successful regression model.

In this work, the quality of reconstruction images is quantitatively evaluated out of visual inspection of artifacts and distortion by calculating the root mean square error (RMSE), coefficient of determination ( $R^2$  score), and image correlation coefficient (ICC) indices among the predicted and true conductivities.

$$RMSE = \sqrt{\frac{1}{N} \sum_i^N (y_i - \hat{y}_i)^2}, \quad (2)$$

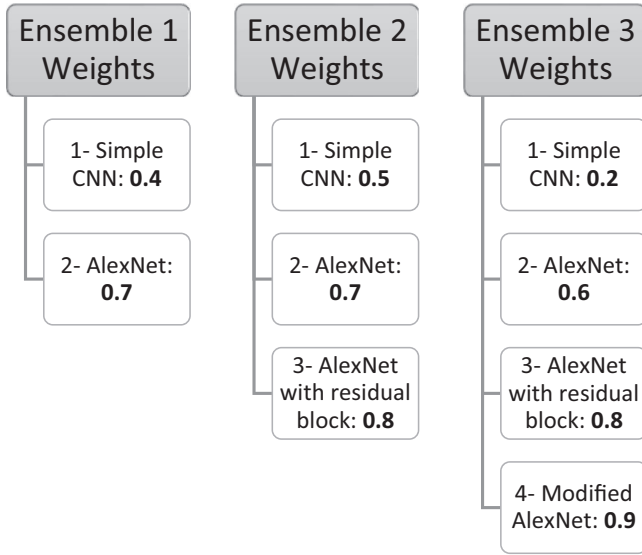


**FIGURE 5** The composition of the first, second, and third ensemble models with the corresponding weight for each model.

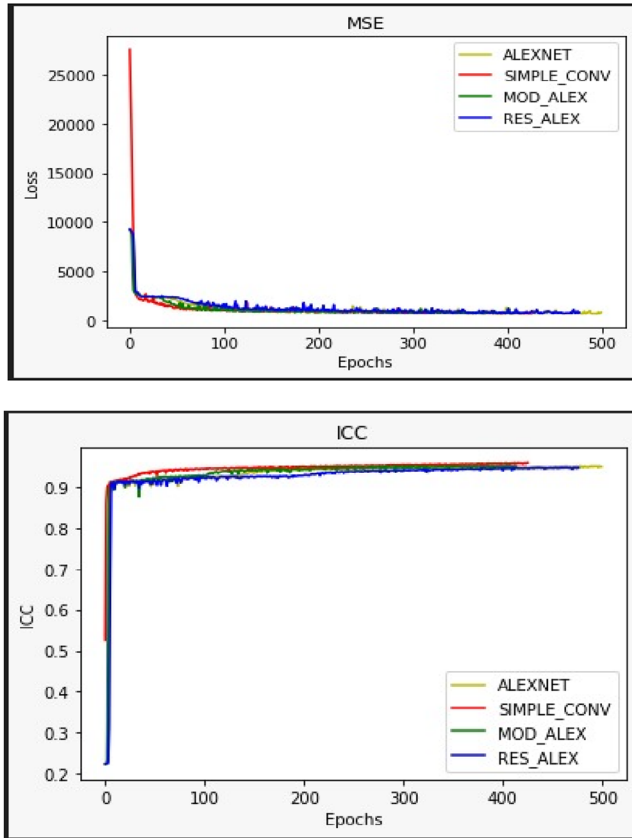


**FIGURE 6** Evaluation standards of simulation dataset during the network training. Comparison of the four proposed models learning curve as a function of the number of epochs. Loss function plot (learning curve) analyzing the behavior of validation losses of five proposed models obtained throughout the training phase.

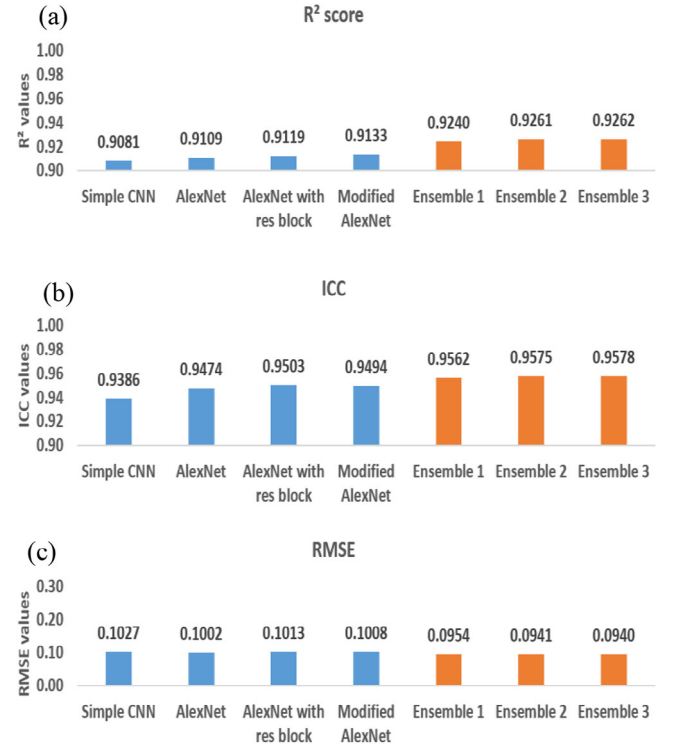


**FIGURE 7** Quantitative analysis for the output of each proposed model from the simulation tests. (a) R<sup>2</sup> score, (b) ICC, and (c) RMSE.

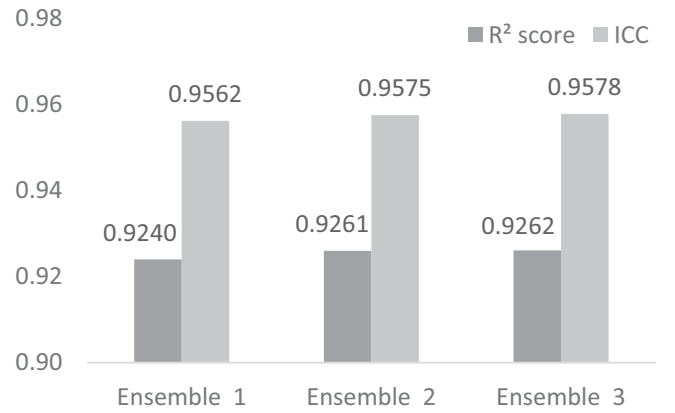


**FIGURE 8** Quantitative analysis for the output of three proposed ensemble models from the simulation tests.

$$R^2 = 1 - \frac{\sum_{i=1}^N (y_i - \hat{y}_i)^2}{\sum_{i=1}^N (y_i - \bar{y})^2}, \quad (3)$$

$$ICC = \frac{\sum_{i=1}^I (y_i^* - \bar{Y}^*) (y_i' - \bar{Y}')}{\sqrt{\sum_{i=1}^I (y_i^* - \bar{Y}^*)^2 (y_i' - \bar{Y}')^2}}, \quad (4)$$

where  $N$  is total number of samples,  $y_i$  is the actual value,  $\hat{y}_i$  is the predicted value, and  $y_i^*$  and  $y_i'$  are also actual and predicted conductivity distributions, respectively.  $\bar{Y}^*$ ,  $\bar{Y}'$  represent the average values of the actual and predicted conductivities, respectively.

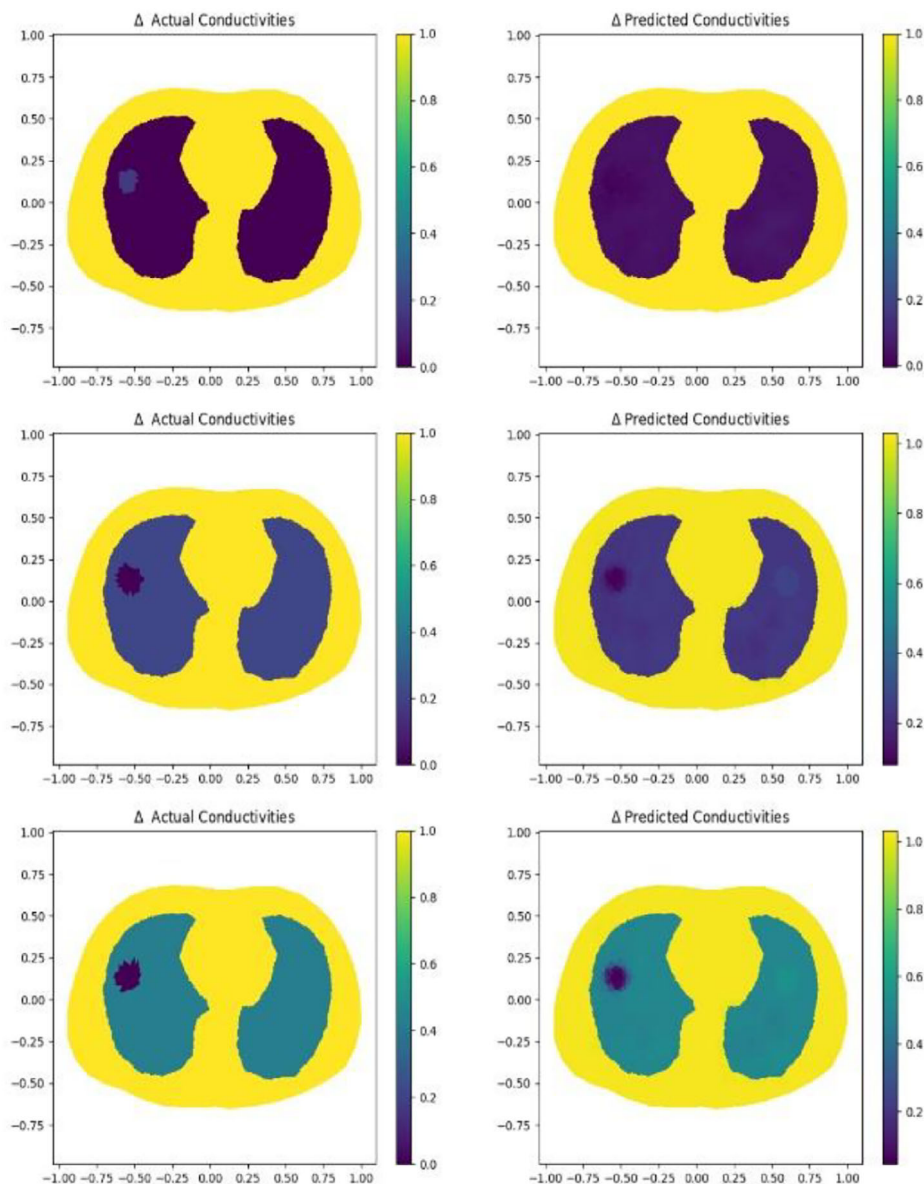


FIGURE 9 Samples of image reconstruction results for the first ensemble model.

For comparison, the RMSE,  $R^2$  score, and ICC values range from zero to one. Whenever the RMSE value is close to zero, this indicates the results of predicted conductivity are accurate. On the other hand, the  $R^2$  score, and ICC can be viewed as a comparison of the true and predicted conductivity. The better model predictions are when the  $R^2$  score and ICC values are closer, which means obtaining accurate image quality and edge-preserving performance.

### 3 | RESULTS AND DISCUSSION

Datasets for training and validation were created and used to train the four proposed CNN architectures. After training, the CNNs were tested and evaluated with the validation dataset. The outputs of all CNN architectures were compared.

In the second stage, the ensemble learning method was applied in three different combinations. For each model, all combinations of the weights with a step of 0.1 are calculated and then the best combinations of weights that achieved the highest  $R^2$  value were chosen. All models are assigned different weights defining the importance of each model for prediction. Based on the theory of trial and error in trying several weights in each experiment and reviewing the results, the appropriate weights are chosen based on the weights that obtained better results and higher accuracy. The weighted average or weighted sum ensemble is an extension over voting ensembles that assume all models are equally skillful and make the same proportional contribution to predictions made by the ensemble. Figure 5 below shows the calculated weights for each proposed method.

The results of image reconstruction based on assigned numerical models and simulation measurements are presented

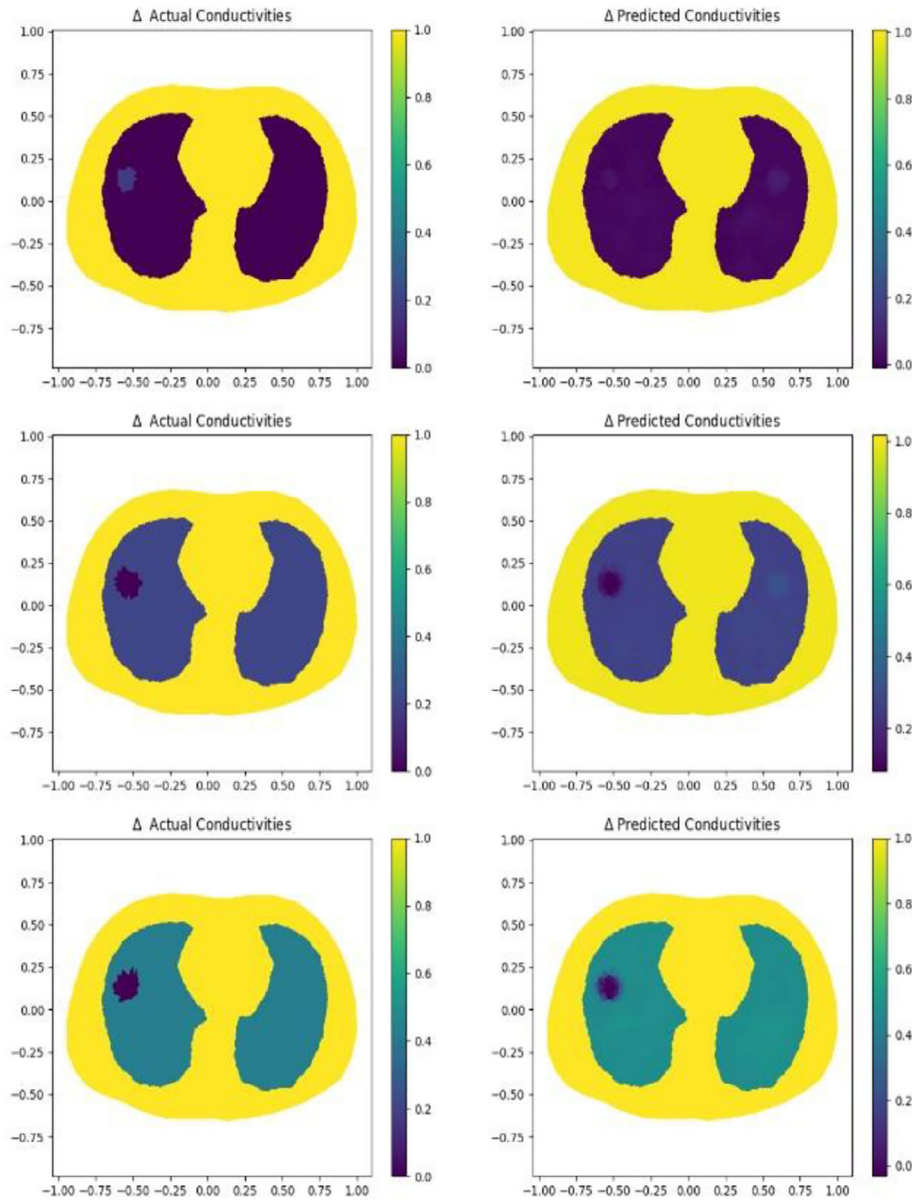


FIGURE 10 Samples of image reconstruction results for the second ensemble model.

in this section. The obtained results were graphically illustrated, allowing for visual analysis of the processes occurring within the object and the use of numerical indicators.

The network output is considered as the estimate of the conductivity distribution for image reconstruction. The suggested approaches were evaluated quantitatively as well as qualitatively. All the metrics shown in this section were computed by running the methods with the set of data saved for testing purposes. The results demonstrate that the proposed framework is effective in improving the quality of reconstructed images.

### 3.1 | Loss curve and evaluation criteria

As appears in Figure 6, with iterations in the network training process, the general trend of the four CNN models is

that RMSE is gradually decreasing, while ICC is constantly increasing.

As the four graphs of the MSE show the simple convolution model is the fastest to converge that makes sense as it has a simple architecture so it would take fewer epochs for it to be trained, but the same can't be said for the rest of the models they take a lot of epochs to train and a lot of time to train but they reach lower losses.

Oscillations can also be seen while training the model. They appear more here on the validation set. This is because the validation set is small, so any small noise while updating the weights of the model has a huge impact on the validation, especially when it has a complicated architecture. Most of the above is also true for the ICC metrics figure, as the simple convolution model converges faster but other models have higher ICC but converge slower.



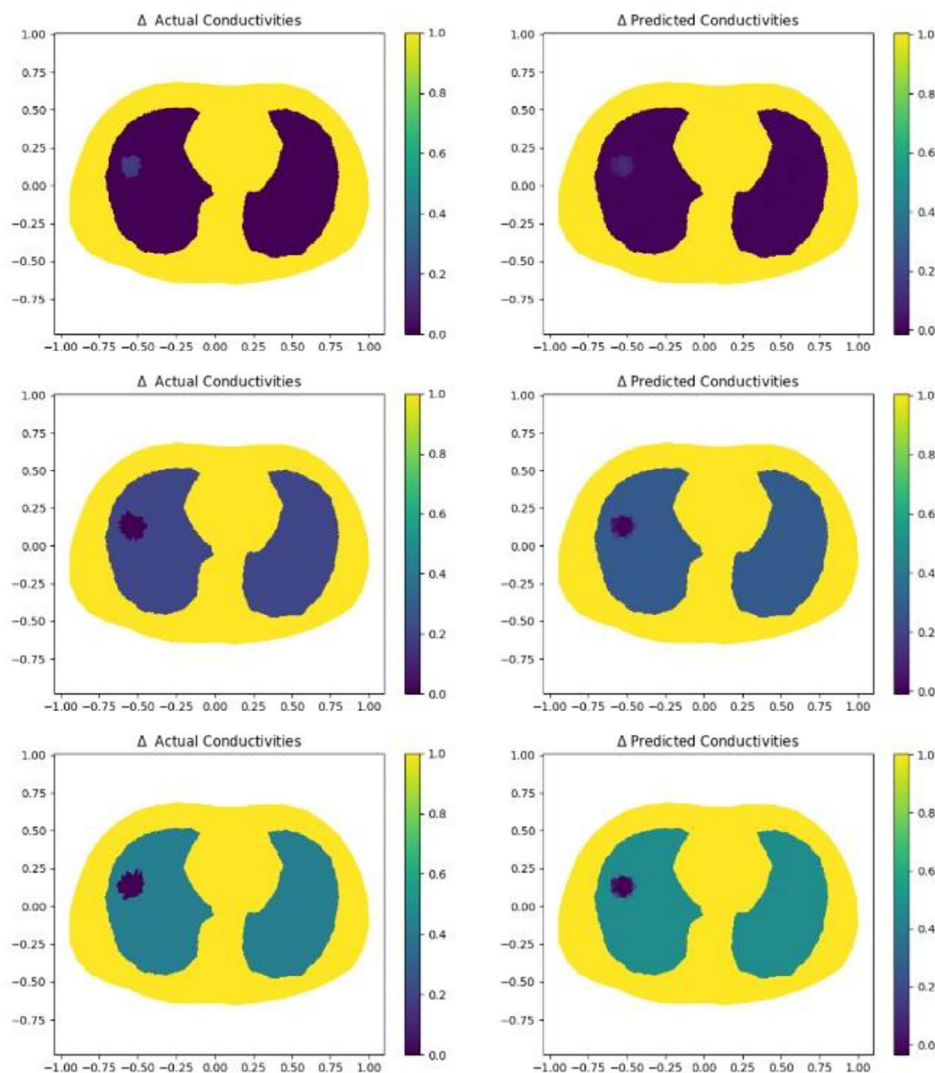


FIGURE 11 Samples of image reconstruction results for the third ensemble model.

The following four bar graphs are a comparison between all proposed models including the ensemble technique after the training process. These results are achieved on both testing and validation datasets to give more accurate measurements for proposed models. In each graph, the individual models are explained first before the ensemble models.

As shown in Figure 7, the obvious feature is the rise in the values of both  $R^2$  and ICC. On the other hand, the RMSE values decrease significantly with the use of ensemble learning.

In close consideration of these results, we notice the clear difference in the evaluation metrics between the use of the individual models in the beginning and then the use of the ensemble models. In contrast, the use of the ensemble technique showed its ability to achieve better results and lower RMSE values.

Within these outcomes, we note no significant difference between the results of ensembles two and three. This is due to several reasons. First, the same type of model was used, which is AlexNet, with some changes in the model implementation. Second, the ensemble approach can be considered as a system that

aggregates several models, therefore increasing the number of models, the accuracy of the ensemble model will increase. But at a certain stage, the system reaches a point of sufficiency. In other words, no matter how many models are there, the accuracy will not increase, and the error will not decrease significantly.

As a summary, the three proposed ensemble models were compared in terms of  $R^2$  and ICC as shown in Figure 8. The results demonstrate that adding a new model with high accuracy contributes to raising the  $R^2$  and ICC scores of the results and reducing the error as the results of the latest model showed which is ensemble three.

### 3.2 | Image reconstruction with simulation data

As mentioned earlier, EIT is a visualization method that uses a series of measurements along the sample boundary to reconstruct the conductivity distribution within an object.

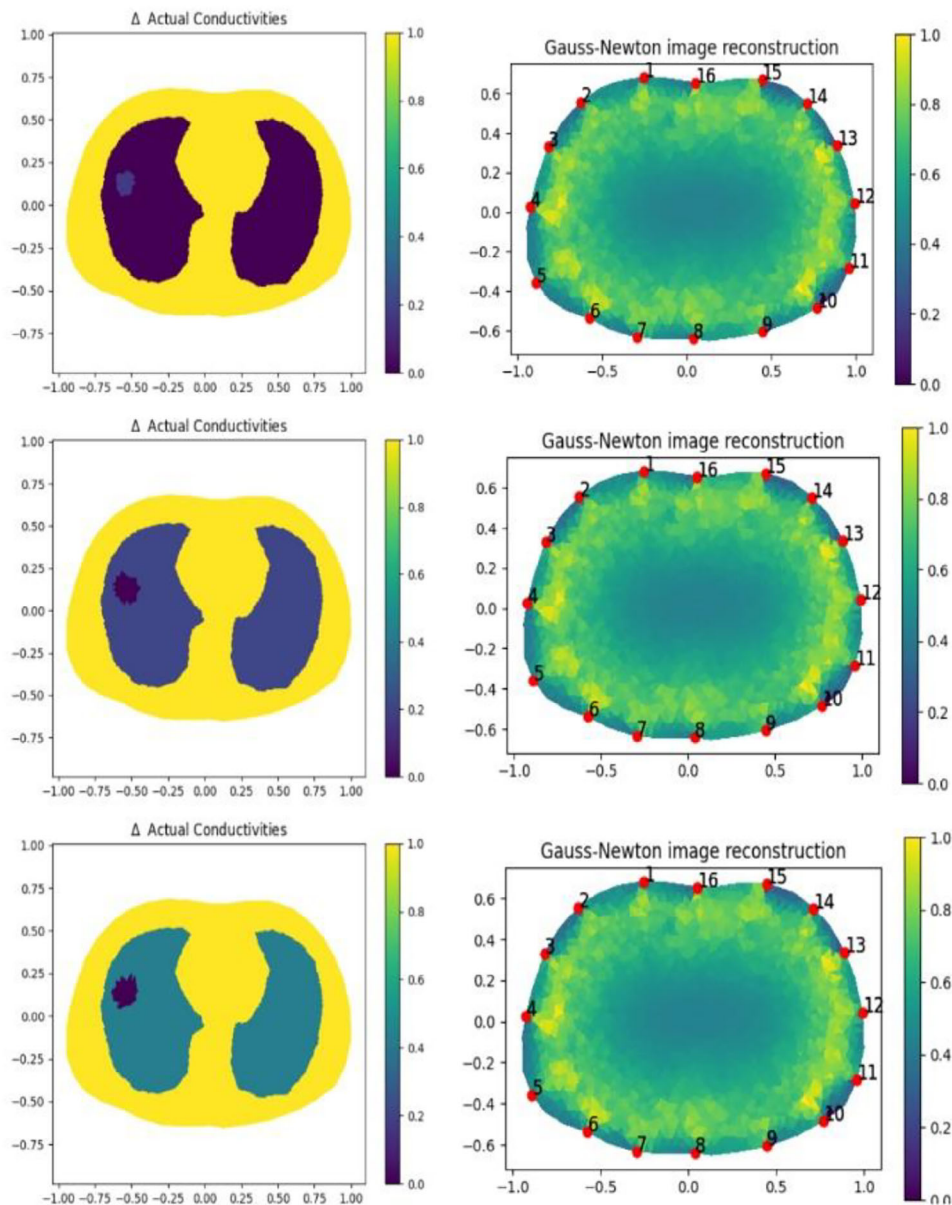


FIGURE 12 Samples of image reconstruction results for the static Gauss-Newton algorithm.

The rainbow-color scheme is a common way to visualize EIT images. The color bar is done automatically, it takes the values of conductivity and assigns a color to each value. The rainbow-color scheme uses bright colors for the highest relative conductivities and dark colors for the lowest relative conductivities.

The left side of the following reconstruction image results represents conductivity change patterns used to simulate boundary voltages (ground truth). The reconstruction of the conductivity change based on simulated voltages is shown on the right side. The numerical scales on the color bars give the conductivity in Siemens per meter ( $S\ m^{-1}$ ).

According to the first proposed ensemble model, the results showed the ability of this method to reduce RMSE values and increase both  $R^2$  and ICC values, thus obtaining high-quality

reconstruction images as shown in Figure 9. The findings of the second proposed ensemble indicated more improvement in the output reconstruction images in both quality and accuracy as evidenced in Figure 10. The final proposed model showed the best results compared with each model or ensemble model previously proposed. The reconstruction images of this model are illustrated in Figure 11, with high resolution and quality.

The results of traditional EIT image reconstruction algorithms such as Gauss-Newton, particle swarm optimization, genetic algorithm etc. showed blurry edges and some additional noise appearing on the reconstructed image. Compared with the proposed ensemble learning, the reconstructed images show clear edges with no artifacts or noise generated.

Figure 12 represents the results of some samples using the Gauss-Newton algorithm. The results did not accurately reflect

the actual conductivities, as shown by the reconstructed images, which also showed artifacts, noise, and poor edge-preserving performances. The lung reconstruction was not done correctly or clearly, which cannot accurately depict the multiphase conductivity distributions and shape characteristics of lungs.

Based on the preceding, we can say that the proposed method to solve the EIT image reconstruction problem has proven its strength in achieving good results in terms of the quality of reconstructed images without any noise, in addition to its ability to reflect the actual conductivities.

Comparing our results with other studies [47, 53, 54] that published a work for EIT lung reconstruction, using an adaptive non-convex hybrid total variation (ANHTV) regularization method as in [53] or a new shape reconstruction framework incorporating the B-spline level set (BLS) sparse Bayesian learning (SBL) as in [54], or an improved Convolutional Neural Network (CNN) method was proposed in [47]. We noticed that our results are enhanced compared to these where we got 0.958 and 0.0940 for ICC and RMSE, respectively. In other studies, they got 0.91, and 0.18; 0.93, and 0.16; and 0.892, and 0.082 for ICC and RMSE, respectively. So compared with the existing state-of-the-art approaches trained before, the suggested ensemble method achieves a high ICC and low RMSE, which indicates that the ensemble learning result has higher accuracy and improves the EIT image quality.

## 4 | CONCLUSION

The prime objective of this work was to develop a new method for EIT image reconstruction for lung monitoring. Therefore, a supervised machine learning technique has been proposed which is the ensemble learning method. The ensemble has combined the predictions of several CNNs models using a simulation dataset of the human thorax. The CNNs models that were used in the ensemble were the simple CNN model, AlexNet, AlexNet with residual block, and the modified AlexNet model and they were combined by using the weighted average technique. Compared with the existing conventional algorithms, the suggested method achieves a high ICC,  $R^2$  score, and low RMSE, which indicates that the ensemble learning resulted in higher accuracy. Also, the proposed ensemble method is beneficial in providing accurate images with high quality and with good anomaly identification which may be used in the future for clinical applications. On the other hand, this work relied on the brute force method which calculates all possible possibilities for the weights of the CNN models and thus determines the weights that achieve the best results. This method may need more time, and in the future, it is possible to rely on faster and more intelligent methods in calculating weights for models. Therefore, if an accurate internal conductivity of the lungs and chest cavity is provided, the proposed method can be applied in real clinical scenarios. In future studies, using real data that represents the human thorax shows the presence of real organs such as the lungs, heart, and diaphragm. This can increase the overall efficiency of the models used and thus increase the accuracy of the reconstructed images.

## AUTHOR CONTRIBUTIONS

**Areen K. Al-Bashir:** Methodology; validation; supervision; visualization; writing—original draft; writing—review & editing. **Duha H. Al-Bataiha:** Methodology; software; visualization; writing—original draft. **Mariem Hafsa:** Methodology; supervision; data curation; visualization; writing—review & editing. **Mohammad A. Al-Abed:** Methodology; validation; supervision. **Olfa Kanoun:** Supervision; review & editing; resources; funding acquisition.

## ACKNOWLEDGEMENTS

This research has been conducted in the context of the project REACT-EU ELIOT supported by the Saxon Development Bank “SAB” (project number #2420156), and was supported by the German Academic Exchange Service (DAAD) by funds from the Federal Ministry for Economic Cooperation and Development (BMZ) Germany, within the project “Promotion of Higher Education in Biomedical Engineering (PROFILE)” (Grant number #57612192).

## CONFLICT OF INTEREST STATEMENT

The authors declare no conflicts of interest.

## DATA AVAILABILITY STATEMENT

Data is available on request from the authors.

## ORCID

Areen K. Al-Bashir  <https://orcid.org/0000-0002-3548-8304>

## REFERENCES

- Ganguly, D., et al.: Medical imaging: A review. In: International Conference on Security-Enriched Urban Computing and Smart Grid. Springer, Singapore (2010)
- Ganguly, D., et al.: Medical imaging: A review. In: Security-Enriched Urban Computing and Smart Grid: First International Conference, SUComS 2010, Proceedings. Springer, Berlin ((2010))
- Doi, K.: Diagnostic imaging over the last 50 years: Research and development in medical imaging science and technology. *Phys. Med. Biol.* 51(13), R5 (2006)
- Lee, J.S., Gleeson, F.V.: Picture the future: Emerging imaging modalities. *Clin. Med.* 14(6), s95–s99 (2014)
- Fred, H.L.: Drawbacks and limitations of computed tomography: Views from a medical educator. *Tex. Heart Inst. J.* 31(4), 345 (2004)
- Kwong, R.Y., Yucel, E.K.: Computed tomography scan and magnetic resonance imaging. *Circulation* 108(15), e104–e106 (2003)
- Chen, Q., et al.: Ultrasound tracking of the acoustically actuated microswimmer. *IEEE Trans. Biomed. Eng.* 66(11), 3231–3237 (2019)
- Harikumar, R., Prabu, R., Raghavan, S.: Electrical impedance tomography (EIT) and its medical applications: A review. *Int. J. Soft Comput. Eng.* 3(4), 193–198 (2013)
- Bodenstein, M., David, M., Markstaller, K.: Principles of electrical impedance tomography and its clinical application. *Crit. Care Med.* 37(2), 713–724 (2009)
- Brown, B.H.: Electrical impedance tomography (EIT): A review. *J. Med. Eng. Technol.* 27(3), 97–108 (2003)
- Wu, Y., et al.: Electrical impedance tomography for biomedical applications: Circuits and systems review. *IEEE Open J. Circuits Syst.* 2, 380–397 (2021)
- Yang, W., Peng, L.: Image reconstruction algorithms for electrical capacitance tomography. *Meas. Sci. Technol.* 14(1), R1 (2002)
- Bera, T.K., et al.: Thin domain wide electrode (TDWE) phantoms for Electrical Impedance Tomography (EIT). In: Proceedings of the 2015



- Third International Conference on Computer, Communication, Control and Information Technology (C3IT). IEEE, Piscataway (2015)
14. Zhao, S., et al.: The impact of the measurement accuracy and the excitation pattern on EIT image reconstruction. In: 2013 6th International Conference on Biomedical Engineering and Informatics. IEEE, Piscataway (2013)
  15. Hao, Z., et al.: Optimal distance of multi-plane sensor in three-dimensional electrical impedance tomography. *Comp. Assist. Surg.* 22(1), 326–338 (2017)
  16. Adam, E.E.B., Babikir, E.: Survey on medical imaging of electrical impedance tomography (EIT) by variable current pattern methods. *J. ISMAC* 3(02), 82–95 (2021)
  17. Sun, B., et al.: A new linear back projection algorithm to electrical tomography based on measuring data decomposition. *Meas. Sci. Technol.* 26(12), 125402 (2015)
  18. Santosa, F., Vogelius, M.: A backprojection algorithm for electrical impedance imaging. *SIAM J. Appl. Math.* 50(1), 216–243 (1990)
  19. Vauhkonen, M., et al.: Tikhonov regularization and prior information in electrical impedance tomography. *IEEE Trans. Med. Imaging* 17(2), 285–293 (1998)
  20. Wang, M.: Inverse solutions for electrical impedance tomography based on conjugate gradients methods. *Meas. Sci. Technol.* 13(1), 101 (2001)
  21. Yang, W., et al.: An image-reconstruction algorithm based on Landweber's iteration method for electrical-capacitance tomography. *Meas. Sci. Technol.* 10(11), 1065 (1999)
  22. Islam, M.R., Kiber, M.A.: Electrical impedance tomography imaging using Gauss-Newton algorithm. In: 2014 International Conference on Informatics, Electronics & Vision (ICIEV). IEEE, Piscataway (2014)
  23. Lionheart, W.R.: EIT reconstruction algorithms: Pitfalls, challenges and recent developments. *Physiol. Meas.* 25(1), 125 (2004)
  24. GhasemAzar, M., Vahdat, B.V.: Error study of EIT inverse problem solution using neural networks. In: 2007 IEEE International Symposium on Signal Processing and Information Technology. IEEE, Piscataway (2007)
  25. Hafsa, M., et al.: A genetic algorithm for image reconstruction in electrical impedance tomography for gesture recognition. *tm-Tech. Mess.* 89(5), 310–327 (2022)
  26. Wang, H., et al.: Image reconstruction for electrical impedance tomography using radial basis function neural network based on hybrid particle swarm optimization algorithm. *IEEE Sens. J.* 21(2), 1926–1934 (2020)
  27. Yamashita, R., et al.: Convolutional neural networks: An overview and application in radiology. *Insights Imag.* 9, 611–629 (2018)
  28. Sercu, T., Goel, V.: Dense prediction on sequences with time-dilated convolutions for speech recognition. *arXiv preprint, arXiv:1611.09288* (2016)
  29. Zhang, B., et al.: Ensemble learners of multiple deep CNNs for pulmonary nodules classification using CT images. *IEEE Access* 7, 110358–110371 (2019)
  30. Alsubibany, S.A., et al.: Ensemble of deep learning based clinical decision support system for chronic kidney disease diagnosis in medical internet of things environment. *Comput. Intell. Neurosci.* 2021, 1–13 (2021)
  31. Sagi, O., Rokach, L.: Ensemble learning: A survey. *Wiley Interdiscip. Rev.: Data Min. Knowl. Discov.* 8(4), e1249 (2018)
  32. Matloob, F., et al.: Software defect prediction using ensemble learning: A systematic literature review. *IEEE Access* 9, 98754–98771 (2021)
  33. De Stefano, C., et al.: A Bayesian approach for combining ensembles of GP classifiers. In: *Multiple Classifier Systems: 10th International Workshop, MCS 2011, Proceedings 10*. Springer, Berlin (2011)
  34. Rokach, L.: Taxonomy for characterizing ensemble methods in classification tasks: A review and annotated bibliography. *Comput. Stat. Data Anal.* 53(12), 4046–4072 (2009)
  35. Rodriguez, J.J., Kuncheva, L.I., Alonso, C.J.: Rotation forest: A new classifier ensemble method. *IEEE Trans. Pattern Anal. Mach. Intell.* 28(10), 1619–1630 (2006)
  36. Mendes-Moreira, J., et al.: Ensemble approaches for regression: A survey. *ACM Comput. Surv.* 45(1), 1–40 (2012)
  37. Lacy, S.E., Lones, M.A., Smith, S.L.: A comparison of evolved linear and non-linear ensemble vote aggregators. In: 2015 IEEE Congress on Evolutionary Computation (CEC). IEEE, Piscataway (2015)
  38. Polikar, R.: Ensemble learning. In: *Ensemble Machine Learning: Methods and Applications*, pp. 1–34. Springer, New York (2012)
  39. Dong, X., et al.: A survey on ensemble learning. *Front. Comput. Sci.* 14, 241–258 (2020)
  40. Pintelas, P., Livieris, I.E.: Special issue on ensemble learning and applications. *Algorithms* 13(6), 140 (2020)
  41. Bashir, S., Qamar, U., Khan, F.H.: IntelliHealth: A medical decision support application using a novel weighted multi-layer classifier ensemble framework. *J. Biomed. Inf.* 59, 185–200 (2016)
  42. Mienye, I.D., Sun, Y., Wang, Z.: An improved ensemble learning approach for the prediction of heart disease risk. *Inf. Med. Unlocked* 20, 100402 (2020)
  43. Shanbhag, G.A., et al.: Prediction of lung cancer using ensemble classifiers. *J. Phys. Conf. Ser.* 2161, 012007 (2022)
  44. Lei, J., Liu, Q., Wang, X.: Ensemble learning-based computational imaging method for electrical capacitance tomography. *Appl. Math. Modell.* 82, 521–545 (2020)
  45. Olberg, S., et al.: Ensemble learning and personalized training for the improvement of unsupervised deep learning-based synthetic CT reconstruction. *Med. Phys.* 50(3), 1436–1449 (2023)
  46. Bader, O., et al.: Two-dimensional forward modeling for human thorax imaging based on electrical impedance tomography. In: 2021 International Workshop on Impedance Spectroscopy (IWIS). IEEE, Piscataway (2021)
  47. Wu, Y., et al.: Shape reconstruction with multiphase conductivity for electrical impedance tomography using improved convolutional neural network method. *IEEE Sens. J.* 21(7), 9277–9287 (2021)
  48. Li, X., et al.: One-dimensional convolutional neural network (1D-CNN) image reconstruction for electrical impedance tomography. *Rev. Sci. Instrum.* 91, 124704 (2020)
  49. Alom, M.Z., et al.: The history began from alexnet: A comprehensive survey on deep learning approaches. *arXiv preprint, arXiv:1803.01164* (2018)
  50. Chen, D., et al.: Deep residual learning for nonlinear regression. *Entropy* 22(2), 193 (2020)
  51. Ma, L., et al.: Deep learning in remote sensing applications: A meta-analysis and review. *ISPRS J. Photogramm. Remote Sens.* 152, 166–177 (2019)
  52. Zhang, Y., Liu, J., Shen, W.: A review of ensemble learning algorithms used in remote sensing applications. *Appl. Sci.* 12(17), 8654 (2022)
  53. Shi, Y., et al.: An adaptive non-convex hybrid total variation regularization method for image reconstruction in electrical impedance tomography. *Flow Meas. Instrum.* 79, 101937 (2021)
  54. Wu, Y., et al.: Bayesian shape reconstruction using B-spline level set in electrical impedance tomography. *IEEE Sens. J.* 22(19), 19010–19019 (2022)

**How to cite this article:** Al-Bashir, A.K., Al-Bataiha, D.H., Hafsa, M., Al-Abed, M.A., Kanoun, O.: Electrical impedance tomography image reconstruction for lung monitoring based on ensemble learning algorithms. *Healthc. Technol. Lett.* 11, 271–282 (2024). <https://doi.org/10.1049/htl2.12085>